International Journal of Science and Research (IJSR)
ISSN (Online): 2319-7064
Index Copernicus Value (2013): 6.14 | Impact Factor (2013): 4.438

Effect on Nanostructured Hydroxyapatite by %TiO_2

Dora E. Ledesma-Carrión[1]

[1]Departamento de Ingeniería en Metalurgia,Escuela Superior de Ingeniería Química e Industrias Extractivas,
Instituto Politécnico Nacional UPALM-Zacatenco, C.P. 07738, México, D.F. MÉXICO. Tel/Fax: 52-55-56100610

Abstract: ***Nanometer and stoichiometric hydroxyapatite was prepared by precipitation of precursors. Later, TiO_2 was added to observe its effect. Different percentages were tested: 0.1, 1.5, 1, 5 and 10, like first approaching. Results show that around 5% appears evidence of a new bond. SEM-HR shows morphology change at 7%, the optimal percentage is between 5 and 7%.***

Keywords: bond, nanostructure, hydroxyapatite, pore size, particle size.

1. Introduction

Hydroxyapatite (HA,$Ca_5(PO_4)_3(OH)$) has hexagonal-bipyramidal symmetry and its properties depend on the synthesis method. The synthetic HA is produced by the precipitation of precursors [1]. The addition of TiO_2 to the HA was carried out in order to improve the mechanical properties because of a new bond. As result of the different experimental technologies there is evidence that around of 5% of TiO_2 it finds the optimal one to reduce the porosity and there is diffusion of titanium on hydroxyapatite.

2. Experiment Details

The average particle size was measured in a Zetasizer nano-Z5 analyzer. Samples consist in 0.01g HA and %TiO_2 diluted each one in 20ml alcohol and subjected to ultrasonic vibration for 30min before measurements were made. The Raman normal vibration modes were measured with Spectrometers Nicolet Almega XR Dispersive Raman Thermo Electron Corporation (laser 532nm, 100% power) and IR modes were studied with Nicolet Nexus 670 FT-IR Thermo Electron Corporation OMNIC (KBr 99% HA 1%), HA + %TiO_2 pills were 1cm of diameter and 0.1g and FT-IR/FT-NIR Perkin Elmer (filters film and KBr). The morphology and chemical compound were observed in powder samples through SEM Stereoscan 440 (20 KV, 250 pA) and SEM-HR FEI Quanta 3D FEG (10 KV, 93.3 pA, x75000). Also, a TEM Jeol JEN 1200 EX (120 KV). XRD Bruker 8 Advance D8 (30 KV, 40mA) and PANalytical X´Pert PRO (45KV, 40mA) were used. The TGA/DSC studies were carried out by a TA-Instruments, model STD Q600, using a standard aluminum pan at a heating rate of 10°Cmin^{-1} on air from 20°C up to 695°C temperature range. Porosity was studied with a BET-BJH test. This study was performed in Minisorp II BEL-Japan with an activation temperature of 110°C in vacuum. Isothermal at 77K for 24h.

For analysis and calculi was used Langmuir adsorption equation. Later statistic analysis was applied to data. XPS tests bonding energies are measure in Thermo Scientific k-alpha Al-Kα 1486.6eV. Pass energy 100eV, charge compensating, dwell time 50ms, chamber pressure 10^{-8} mbars, analysis area 400μ^2, angle 90°C, resolution 0.5eV and reference C 2s. Raman-HR tests were measure in Lab Ram HR800 Horiba Jobin Yvon, frecuencies 532cm^{-1} and 633 cm^{-1}. Ellipsometry tests were measurement in UVISEL LT M200 AGMS Horiba Jobin Yvon (Xe 75W, spectral range: 1.5- 5.5eV or 150-900nm).

3. Results and Discussion

TGA/DSC tests were applied to HA with/without heat treatment (HAcc/HAsc) and %TiO_2:

Phase transforms of TiO_2 are observed in Figure 1: Anatase at 480°C and rutile at 580°C. Also, the water loss is observed in the first exothermic plateau (positive slope) for HA (Figure 2).

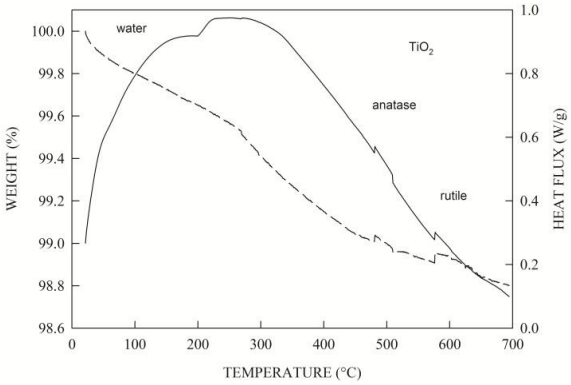


Figure 1: TGA/DSC test: Phases of TiO_2, anatase and rutile, are observed at 480°C and 580°C, respectively.

Figure 2a shows that the temperature which one started forming the HA is at 300°C and in which it starts crystallizing at 475°C for the HA without heat treatment. For HA with heat treatment, figure 2b, does not appear the water curve and HA is crystallized.

Comparing TGA tests for HAcc + %TiO_2 is showed in figure 3. Carbonate zone begins at 700°C up to 850°C. Phosphates zone begins at 900°C. The most thermal stability is in 5% of TiO_2. Comparing DSC for HAcc + %TiO_2 is showed in figure 4.

Licensed Under Creative Commons Attribution CC BY

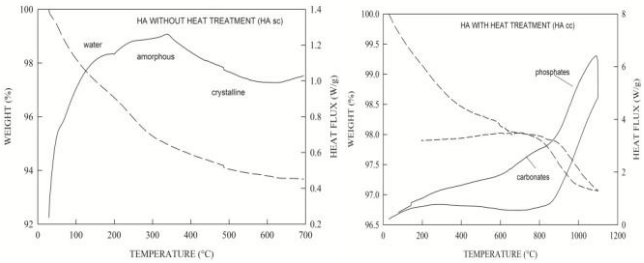


Figure 2: TGA/DSC test: a) HA sc begins to crystallize at 475°C and b) HAcc which one is crystalline and break down in carbonates and phosphates at 700°C and 900°C, respectively.

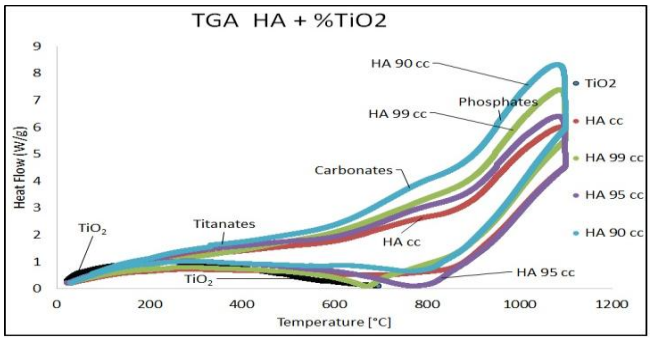


Figure 3: TGA tests HAcc + %TiO_2 show same carbonate and phosphates zones for each percentage of dioxide of titanium.

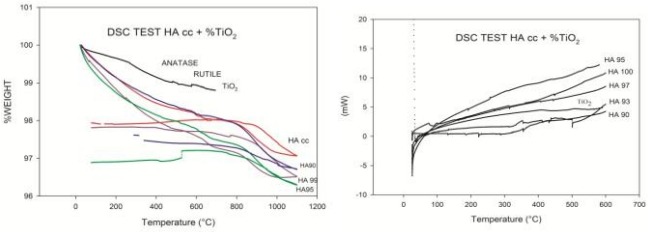


Figure 4: HAcc + %TiO_2 DSC test shows peaks displacement corresponding to anatase and rutile TiO_2 phases. There is more thermal stability in 5%TiO_2 than others percentages. a) DSC plots in weight in percentages and b) Weight in absolute values.

For major percentage of dioxide of titanium the phase changes are more visible and in the curve of hysteresis there is a displacement. In case of 1%TiO_2 there is between 600°C and 750°C in the curve of hysteresis. Whereas that the same peak appears between 700°C and 850°C for 5 and 10%TiO_2. This peak would correspond to the anatase phase since the XRD like that verified it, this is, rutile phase is no present, such as it is showed in figure 5.

In case of 5% the peak is thinner and the minimum appears to one %weigth more under than in case of 10% of dioxide of titanium. These materials are considered pure. The effect of the addition of dioxide of titanium to HA with heat treatment displaces the temperature of phase change.

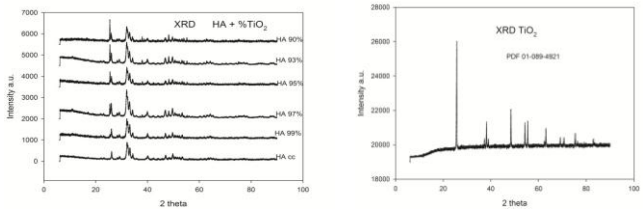


Figure 5: Comparative number of patients for male and female by age group for base scenario and minimum initial value.

On the other hand the HAcc XRD pattern showed a stoichiometric compound with a single phase (PDF 89-4405). For HAcc + %TiO_2 in all patterns do not appear CaO plane (200) pick, thus, there is not HA contamination or breakdown with treatment, this can be observed in figure 6. HA is reported with CaO plane pick (Afshar et al 2003, Yeong et al 1999, 2001, Mostafa et al 2005 and Juang et al 1995) arguing that the FTIR results show an intense carbonate band (ν_3 carbonate bands 1450-1550 cm^{-1}). So, in order to reach a pure HA precipitate with traces of carbon dioxide contamination, it is effective to use controlled atmosphere during precipitation process.

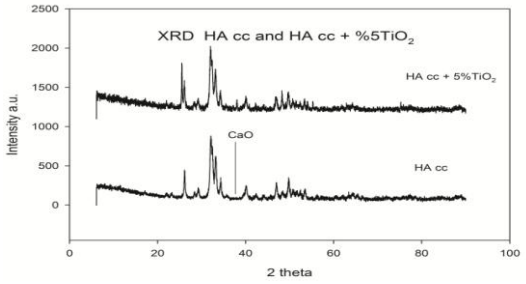


Figure 6: HAcc and HA + 5%TiO_2 diffraction patters do not observe CaO plane or rutile phase.

To verify pore size in a nanometer range in figure 7 and tables 1 and 2 appear Nitrogen-Adsorption-desorption (BET/BJH) tests. Those showed mesoporosity (curves type II, (Sing et al 1985 and Condon et al 2000)) with a total surface area of 37.8m2/g, pore volume V_p of 0.061055cm^3/g for HAcc. The BET tests results showed total surface area reducing 8.93% when percentage of TiO_2 were increasing up to 10% and the reduced maximum corresponding to 5%TiO_2. The BJH test results show V_p (pore volume), $r_{p,peak}$ (peak pore radii) and a_p (pore area) increased to 13.8% and 54.1% when percentage of TiO_2 were increasing up to 10% and the a_p does not show trend, respectively. (Sing et al, 1985 and Rouquérol *et al*, 1994).

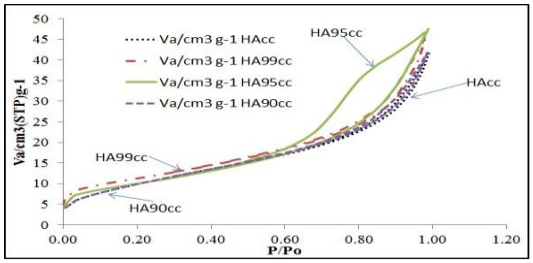


Figure 7: BET tests HAcc + %TiO_2 show mesoporosity for each percentage of dioxide of titanium. The smallest porosity is in 5%TiO_2.

Licensed Under Creative Commons Attribution CC BY

Table 1: HAcc + %TiO_2 BET tests show reduced total area.

BET analysis HA cc + $\%TiO_2$.		
	area [m^2/g]	
HA cc 100% cc	37.8	0.26%
HA cc 99%$TiO_2$1%	37.9	−8.44%
HA cc 95%$TiO_2$5%	34.7	8.93%
HA cc 90%$TiO_2$10%	37.8	

Table 2: HAcc + %TiO_2 BJH tests show pore volumen, peak radii and area.

Plot data	HA cc	Adsorption branch	
V_p		0.061055	$[cm^3g^{-1}]$
$r_{p,peak}$(Area)		1.22	[nm]
a_p		32.53	$[m^2g^{-1}]$
Plot data	1%TiO_2	Adsorption branch	
V_p		0.064385	$[cm^3g^{-1}]$
$r_{p,peak}$(Area)		1.66	[nm]
a_p		30.429	$[m^2g^{-1}]$
Plot data	5%TiO_2	Adsorption branch	
V_p		0.069464	$[cm^3g^{-1}]$
$r_{p,peak}$(Area)		1.88	[nm]
a_p		31.243	$[m^2g^{-1}]$

To verify the maximum mesoporosity correspond to 5% dioxide of titanium figure 7 shows BET tests analysis. And particles average size distribution, figure 8 show that for TiO_2 is 294nm, HAcc is 175.9nm, 5%TiO_2 is 293.6nm and 10% is 206.4nm. In 5%TiO_2 the distribution is 2-modal whereas others are 1-modal, such that titanium spread in HA.

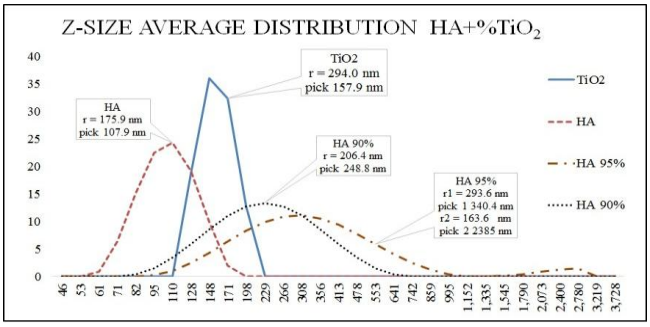


Figure 8: Z-Size Average Distributions show 1-modal forms for HAcc, 10% and TiO_2, and 2-modal for 5%.

The HAcc + %TiO_2 rod-like and changing morphology and chemical compound were verified by scanning and transmission electron microscopes results and presented in figures 9 and 10. These results showed a particle size ranging from 20 to 200nm. SEM-HR micrograph (from x15000 to x150000) indicates that the precipitated particles have a changing morphology from rod-like morphology with ~100nm in lateral and ~20nm in diameter dimensions (HA cc) to rod-like and spheres for 5% and after rod-like with small cluster for 7%. HAcc TEM-HR micrograph shows hexagonal nanostructure. It is showed in figure 11.

Morphology changing is because of heat treatment applied to HA after dried process. In this process the powder was heated for 3h at 680°C using argon atmosphere from 500°C to 680°C with initial and terminal temperature rate of 10°C/min.

HAcc + %TiO_2 Raman and IR spectra evidence presence of titanium spreading in the HA matrix. Beginning at 1% and finished before of 10%.

To verify Raman spectra results figure 13 shows Rama HR results. The same effect of TiO_2 in HAcc appears on 5 and 7%. Hydroxyl group disappears from 3%TiO_2 up to 10%. So there is one titanate, carbonate or phosphate possible bond in watery media.

TiO_2([3], [4]) ν_1 absorption band appears at 600-700cm^{-1} and 525-460cm^{-1}, ν_2 band is at 380-329cm^{-1} and ν_3 band is at 185-91cm^{-1} and 100-91cm^{-1}.

Synthetic HA [2] hydroxyl band is observed at 3568cm^{-1}. Phosphate band, ν_1, is in region from 473 to 410cm^{-1} with a site at 436cm^{-1}, ν_2 phosphate band is at 980-915cm^{-1}, ν_3 is at 1092, 1085 1nd 1052cm^{-1}. ν_4 band is at 658-538cm^{-1}. To verify that there is a bond figure 14 signs XPS tests analysis. It shows 2p Ca (347.5eV, 351.5eV), 1s O (530.5- 531eV), 2p Ti (459.5eV), 2p P (132.5eV) and hydroxyl (531- 532eV) bonding energy. Titanate, Carbonate and phosphate bonding energies are 456.3eV, 531.5-532.5eV and 530.5- 532.9eV, respectively. Like stoichiometric HA pH is 9-10 then strong basic [PO_4^{3-}] ion is present in electrochemical reaction $Ca_5(PO_4)_3(OH) + 5TiO_2 + O_2 \leftrightarrow 5CaTiO_3 + H^+ + 3PO_4^{3-} + 8e^-$ XPS tests for Ha + %TiO_2 powders contain Ca, P, H, O, Ti only, so that material is does not contaminate.

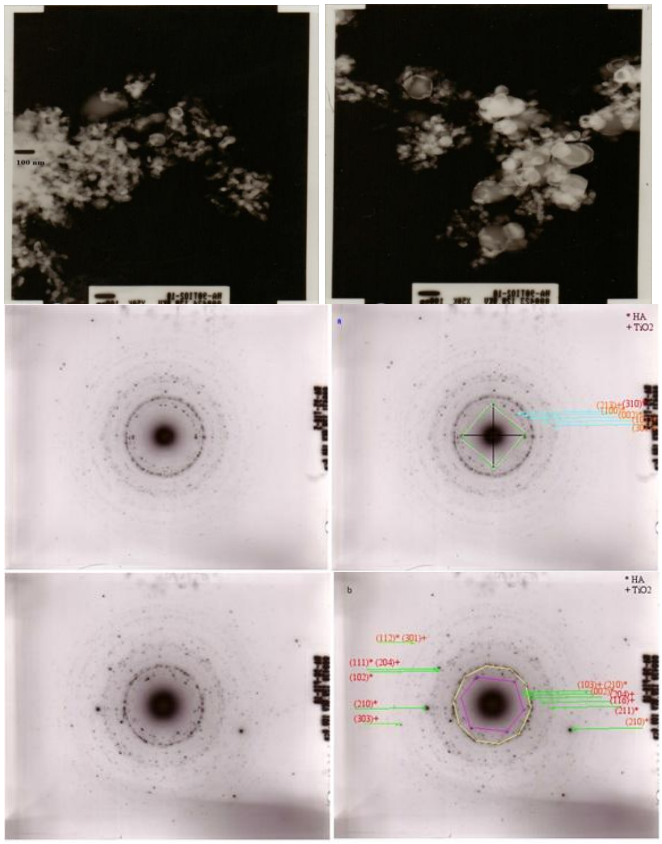


Figure 9: Electron diffraction pattern a) HAcc + 5%TiO_2 TEM micrograph shows nanostructure ~100nm, b) HAcc + 10%TiO_2 TEM micrograph shows particle size ~200nm. Electron diffraction shows nanostructure and lightly textured for, c) HAcc + 5%TiO_2 and d) HAcc + 10%TiO_2.

4. Conclusion

Phases balance appears around 5% of TiO_2 because of particle size similar between two phases, stoichiometric and

Licensed Under Creative Commons Attribution CC BY

pH synthetic HA and changing morphology is observed in 7%TiO_2. So the addition of dioxide of titanium to hydroxyapatite it is not a trend but an optimal percentage. This optimal is between 5% to 7%.

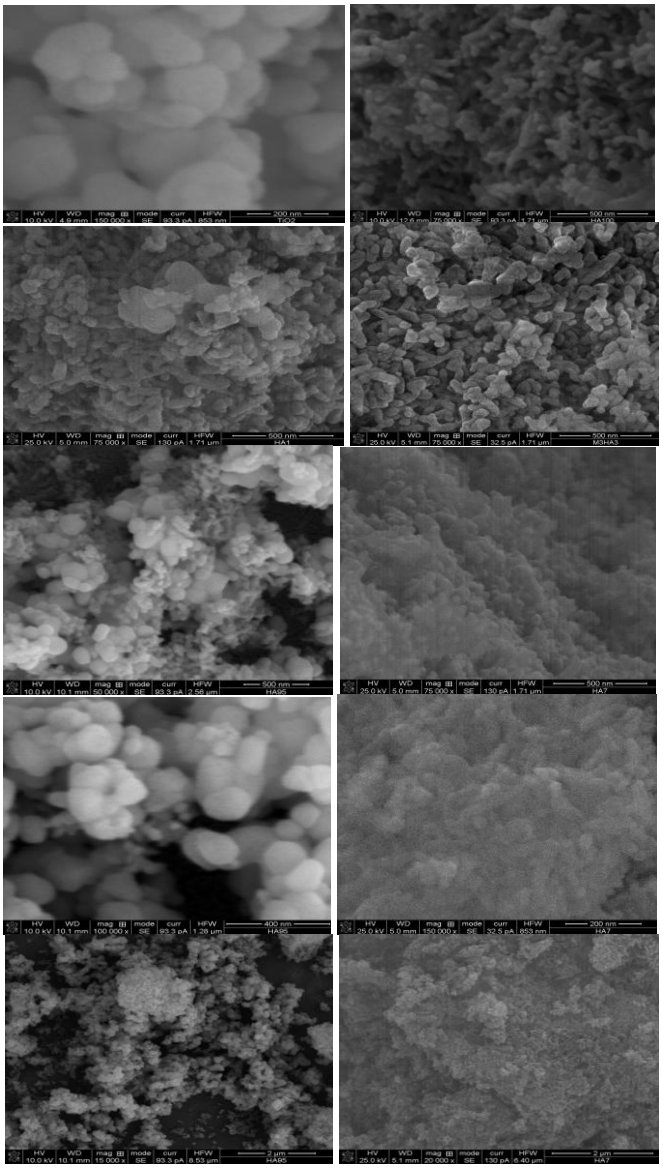


Figure 10: HAcc + %TiO_2 micrographs SEM-HR show morphology changing. This changing begins at 5% and finishes at 7%.

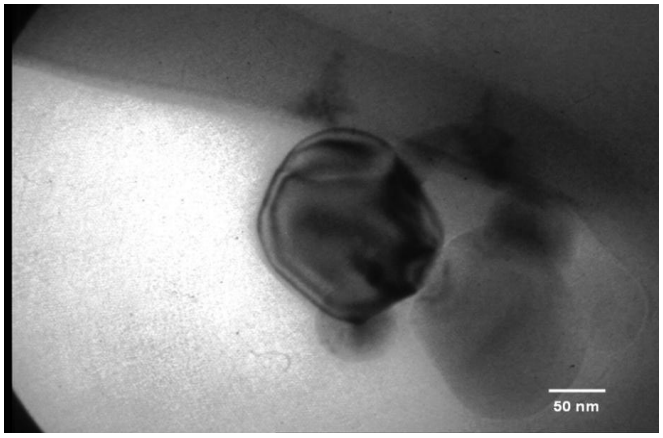


Figure 11: HAcc TEM-HR micrograph shows hexagonal nanostructure and particle size ~100nm.

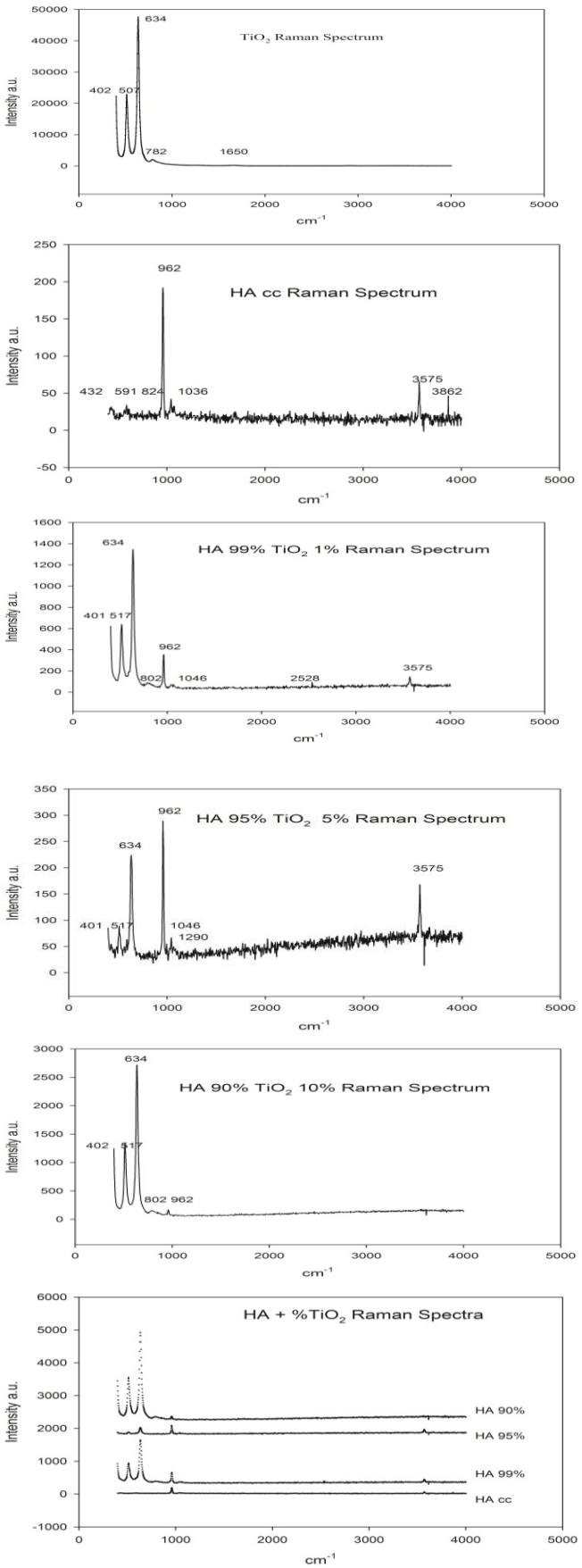
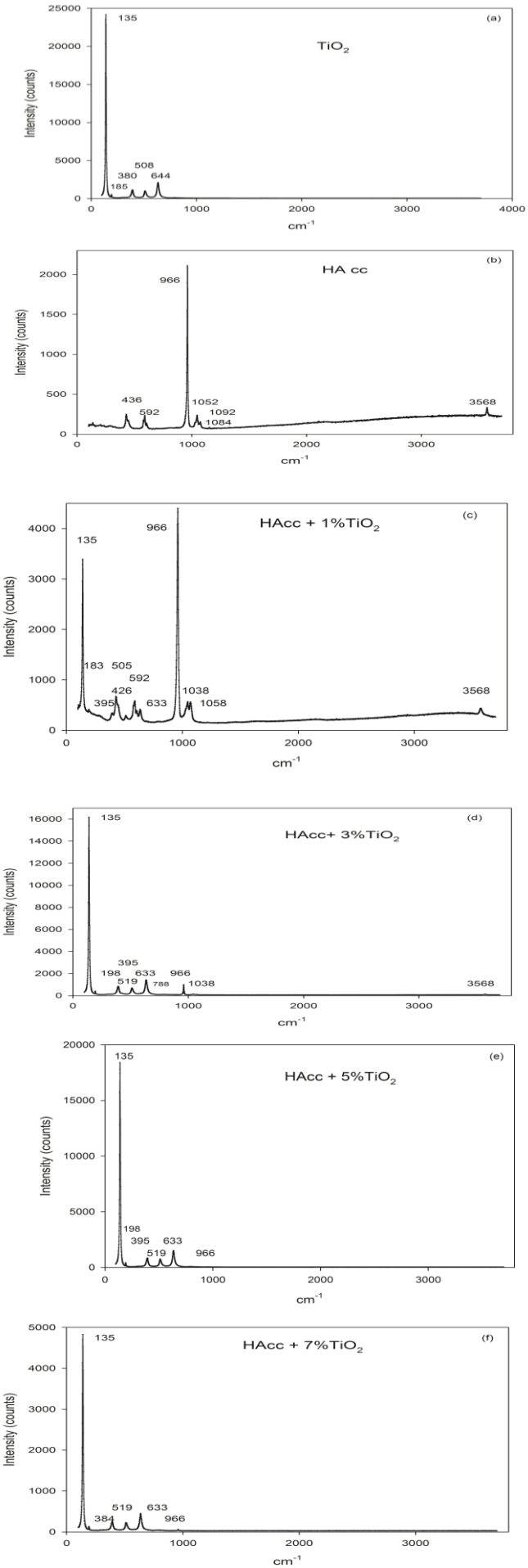


Figure 12: HAcc + %TiO_2 Raman spectra show titanium spreading in HA matrix. This event begins at 5% and finished 7% of TiO_2.

Licensed Under Creative Commons Attribution CC BY



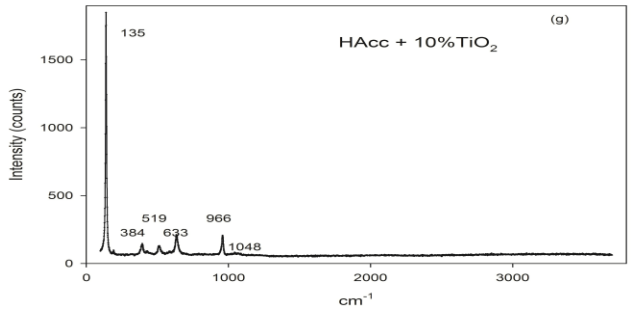


Figure 13: HAcc + %TiO_2 Raman HR spectra show titanium spreading in HA matrix. This effect starts at 5% and finishes at 7% of TiO_2.

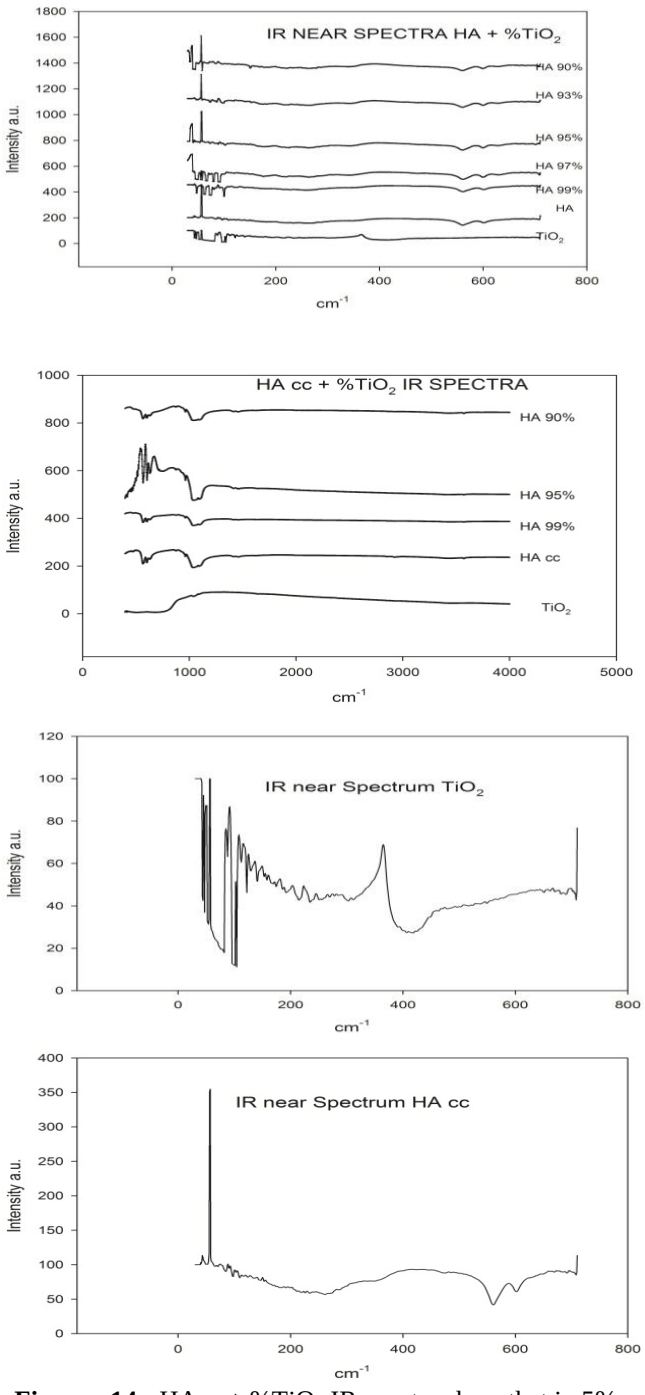


Figure 14: HAcc + %TiO_2 IR spectra show that in 5% as stringer than others percentages.

Licensed Under Creative Commons Attribution CC BY

5. Acknowledgment

This work is partially financially by UNAM-IN109308, CONACyT 80380 projects. Authors would like to thank Centro de Nanociencas y Micro y Nanotecnologías del IPN, Universidad Autónoma del Estado de Hidalgo and PhDs Prof. Heriberto Pfeifer, Martha Teresita Ochoa-Lara, Fidel Pérez-Moreno, Omar Novelo-Peralta, Carlos Flores-Morales, Luis Moreno-Ruiz, Mayahuel Ortega, Hugo Martínez, Juan Méndez-Méndez, Luis Lanturno-Rojas, José Andraca, Israel Arzate-Vazquez, Sc.M. Claudia Ramos-Torres, Jorge Osorio-Fuente, Ana Dueñas-Pérez, M.T.L. Muciño-Porras, Esteban Fregoso and Lidia Hernández-Hernández for your help and support in the characterization process.

References

[1] Ledesma-Carrión Dora E., "Modification on the Synthesis Process of Hydroxyapatite", Proceedings of the international MultiConference of Engineers and Computer Scientists 2015, Vol II, pp.762-766, ISBN: 978-988-19253-9-8, ISSN: 2078-0958 (Print); ISSN: 2078- 0966 (Online), 2015. Prajneshu, "Diffusion approximations for models of population growth with logarithmic interactions," Stochastic Processes and their application, Vol. 10 pp. 87-99, North-Holland Publishing Company, 1980.
[2] Afshar A., Ghorbani M., Ehsani N., Saeri M. R. and Sorrell C. C., Materials & Design, Vol. 24, pp. 197-202, 2003.
[3] Garcia C., Paucar C. and Gaviria J., "Study of some parameters that determine the synthesis of hydroxyapatite by the precipitation route", Dyna rev.fac.nac.minas[online], vol.73, n.148, pp. 9-15, ISSN 0012- 7353, 01/06.
[4] Guzmán C., Pia C. and Munguía N., Rev. Mex. Fis., Vol. 51, pp. 284- 293, 2005.
[5] Juang H. Y. and Hon M. H.,Biomaterials, Vol. 17, pp. 2059-2064, 1995.
[6] Joschek S., Nies B., Krotz R. and Göpferich A., Biomaterials, Vol. 21, pp. 1645-1658, 2000.
[7] Yeong K.C.B., Wang J. and Ng S.C., Biomaterials, Vol. 22, pp. 2705-2712, 2001.
[8] Mostafa N. Y.,Materials Chemistry and Physics, Vol. 94, pp. 333-341, 2005.
[9] Yeong K.C.B., Wang J. and Ng S.C., Materials Letters, Vol. 38, pp.208-213, 1999.
[10] Rehman I. and Bonfield W., Journal of Materials Science: Materials in Medicine, Vol. 8, pp. 1-4, 1997.
[11] Feng-Huei L., Liao Ch. J., Ko-Shao Ch. and Jui-Sheng S., Materials Science and Engineering C, Vol. 13, pp. 97-104, 2000.
[12] Sing K.S.W., Everett D.H., Haul R.A.W., Moscou L., Pierotti R.A., Rouquérol J. and Siemieniewska T.,Pure & Appl. Chem. IUPAC, Vol. 57, No. 4, pp. 603-619, 1985.
[13] Condon J. B., Microporous Mesopourus Mat., Vol. 38, pp. 359-383, 2000.
[14] Rouquérol J., Avnir D., Fairbridge C.W., Everett D.H., Haynes J.H., Pernicone N., Ramsay J.D.F., Sing K.S.W. and Unger K.K., Pure & Appl. Chem. IUPAC, Vol. 66, No. 8, pp. 1739-1758, 1994.
[15] Gómez J., Elizondo N. and Guerrero H., Ingenierías, Vol. 24, pp. 46- 50, 2004.
[16] Neder, N.B. and Proffen, Th., J. Appl. Cryst. Vol. 29, pp. 727-735, 1996. Würzburg Universität.
[17] Briggs, D. and Seah, M.P., John Willey & Son, Vol. 1, second edition, 1993.
[18] Wagner, C.D., Moulder, J.F., Davis, L.E. and Riggs, W.M., Handbook of X-ray photoelectron spectroscopy Perking-Elmer Corporation, Physical Electronic Division.

Author Profile



Dora Elena Ledesma-Carrión received the degree in Physics, M.Sc. and PhD degrees in Engineering from Universidad Nacional Autónoma Nacional de México in 1986, 1997 and 2004, respectively. She has worked in the government institutions from 1986. Also she has advised different companies. Lines of investigation are operations research and materials science.

Licensed Under Creative Commons Attribution CC BY